ADVANCES IN FOREST FIRE RESEARCH

2022

Edited by
DOMINGOS XAVIER VIEGAS
LUÍS MÁRIO RIBEIRO

Will Concentrated Sunlight Ignite a Wildfire?

Shaorun Lin[1], Siyan Wang[2], Yanhui Liu[1], Xinyan Huang[1,*], Michael J. Gollner[2]

[1]Research Centre for Fire Safety Engineering, Department of Building Environment and Energy Engineering, The Hong Kong Polytechnic University, Hong Kong, {flynn.lin@connect.polyu.hk, myname.yanhui@connect.polyu.hk, xy.huang@polyu.edu.hk}
[2]Deparment of Mechanical Engineering, University of California, Berkeley, CA, USA, {siyan_wang, mgollner}@berkeley.edu

**Corresponding author*

Keywords

Smouldering; Point Heating Source; Irradiation Spot; Ignition Energy; Modelling.

Abstract

Concentrated sunlight is a potential ignition source of wildfires, but its ignition mechanism is still poorly understood. Herein, we study the smoldering ignition of tissue paper (a common fuel that was abandoned by human in wildland) by a concentrated sunlight spot with heat fluxes up to 780 kW/m2, which is focused by a transparent glass sphere. The diameter of the sunlight spot on the paper sample ranges from 1.5 to 20.0 mm by varying the paper position within the focal length, where a smaller spot has a larger intensity of sunlight irradiation. We found that the concentrated sunlight can easily ignite the tissue paper. The measured minimum spot irradiation for smoldering ignition is not a constant but is much higher than 11 kW/m2 measured in a traditional cone-calorimeter test. As the diameter of the irradiation spot decreases from 20 to 1.5 mm, the minimum irradiation for smoldering ignition increases from 17.5 to 205 kW/m2. A 2-D computational model was successfully applied to reproduce the experimental observations and validate the results. This work ultimately quantifies the potential fire risk from concentrated sunlight spots and helps elucidate the underlying mechanisms leading to smoldering ignition.

1. Introduction

The ignition of wildland fuels defines the initiation of devastating fire events. Many ignition events leading to wildland fires occur remotely by a point heating source (Caton et al. 2017), such as the deposition of lofted firebrands, lightning strikes, and concentrated sunlights (Fernandez-Pello 2017a; Wang et al. 2022). Significant studies have focused on spotting ignition by lofted firebrands (Fernandez-Pello 2017b). Comparatively, a lesser-studied source of ignition is a concentrated sunlight spot, which can be focused by a dew droplet, curved glass window and decorations, transparent fish bowls, or cylindrical bottles filled with water (Fig. 1a). In 2018, sunlight concentrated by shards of broken glass had burned roughly 80 acres near Reardan, Washington (Fig. 1b). However, our understanding on this potential ignition source is still limited.

Once an intense irradiation spot is applied, a recipient fuel may first be heated, dried, decompose, and then begin to smolder (Drysdale 2011). Smoldering can be easily initiated by a weaker ignition source or even self-ignited, providing a shortcut to severe fire events through the smoldering-to-flaming transition (Rein 2014; Santoso et al. 2019). Therefore, it is of vital significance to fully understand smoldering ignition. So far, little research has studied the smoldering ignition by concentrated irradation spots, and the ignition criteria are still poorly understood.

This work investigates the smoldering ignition of multiple-layered tissue paper samples by sunlight spots concentrated by a spherical glass ball. Within the focus length, the diameter of the heating spot was varied from 1.5 mm to 20 mm, and the intensity of irradiation was varied up to 780 kW/m2. The ignition delay time, critical heat flux of smoldering by the irradiation spot were quantified. Eventually, a 2-D model will be established to vlidate the experimental results.

(a) (b)

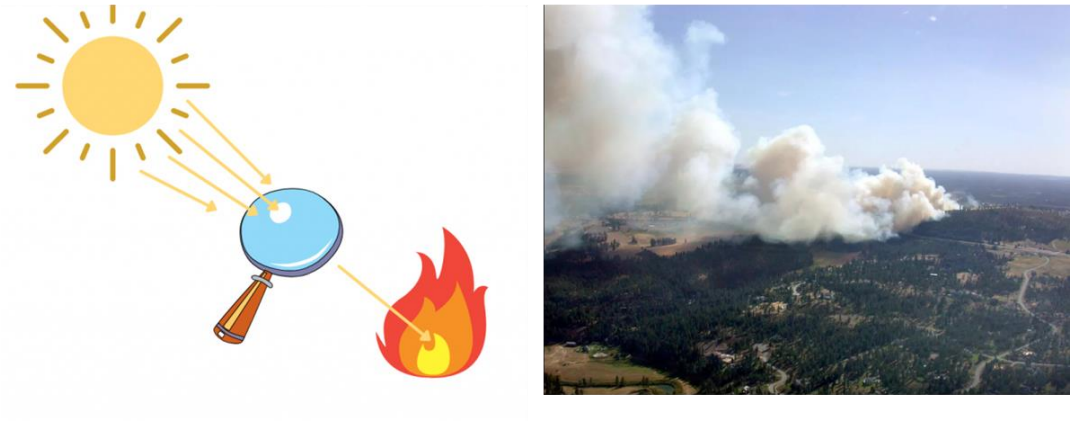

Figure 1- (a) schematic diagram of ignition by concentrated sunlight (copyright: Survival Guide), (b) a wildfire triggered by sunlight concentrated in US (copyright: The Spokesman-Review).

2. Experimental Method

2.1. Materials and setups

Thin tissue paper was used in the experiment, as it was a typical thin fuel abondoned by humans in wildlands. Before the test, the tissue paper was first oven-dried at 75 ℃ for 48 h, and its dried bulk density was measured to be 98 ± 5 kg/m^3. For the test, the tissue was first cut into a size of 60 mm × 60 mm, and six layers of tissue were packed into a sample with an overall thickness (δ) of about 2 mm (see Fig. 2a).

In the experiment, natural sunlight was concentrated by a 150-mm K9 crown glass sphere with a refractive index (n_c) around 1.53. The focal length and back focal length of the crown glass sphere were theoretically calculated to be 108 mm and 33 mm, as illustrated in Fig. 2b.

A solar power meter was fixed at the front towards the sunlight direction to record real-time solar irradiation ($\dot{q}_s''$). The sample frame was a hollow box that was inserted into the sample holder. The sample holder was installed on a slide that can adjust its distance between the tissue sample and the glass sphere with a precision of 0.5 mm.

2.2. Quantification of solar irradiaiton heat flux

To quantify the high irradiation of concentrated sunlight spot, an optical simulation performed in *TracePro* (TracePro) was first used to c orrelate the size of the light spot and theoretical irradiation ($\dot{q}_c''$) concentrated by a 150-mm crown glass sphere.

In the optical simulation, the overall concentration factor (C) is a ratio of irradiation level after and before concentrating which could be used to quantify the concentrated irradiation flux in this study. Fig. 2b shows the overall concentration factor (C) vs. light spot diameter (D) of a 150-mm glass sphere based on an optical simulation performed in *TracePro* (TracePro).

With the instant solar irradiation ($\dot{q}_s''$) and the overall concentration factor (C) for different light spots determined, the actual concentrated solar irradiant heat flux to the fuel sample can be calculated as

$$\dot{q}_c'' = C\dot{q}_s'' \qquad (1)$$

Four different positions (x) of 3 mm, 13 mm, 19 mm, and 33 mm within the glass sphere's back focal length were tested, with respect to four heating diameters (D) of 20.0 mm, 9.0 mm, 5.5 mm, and 1.5 mm.

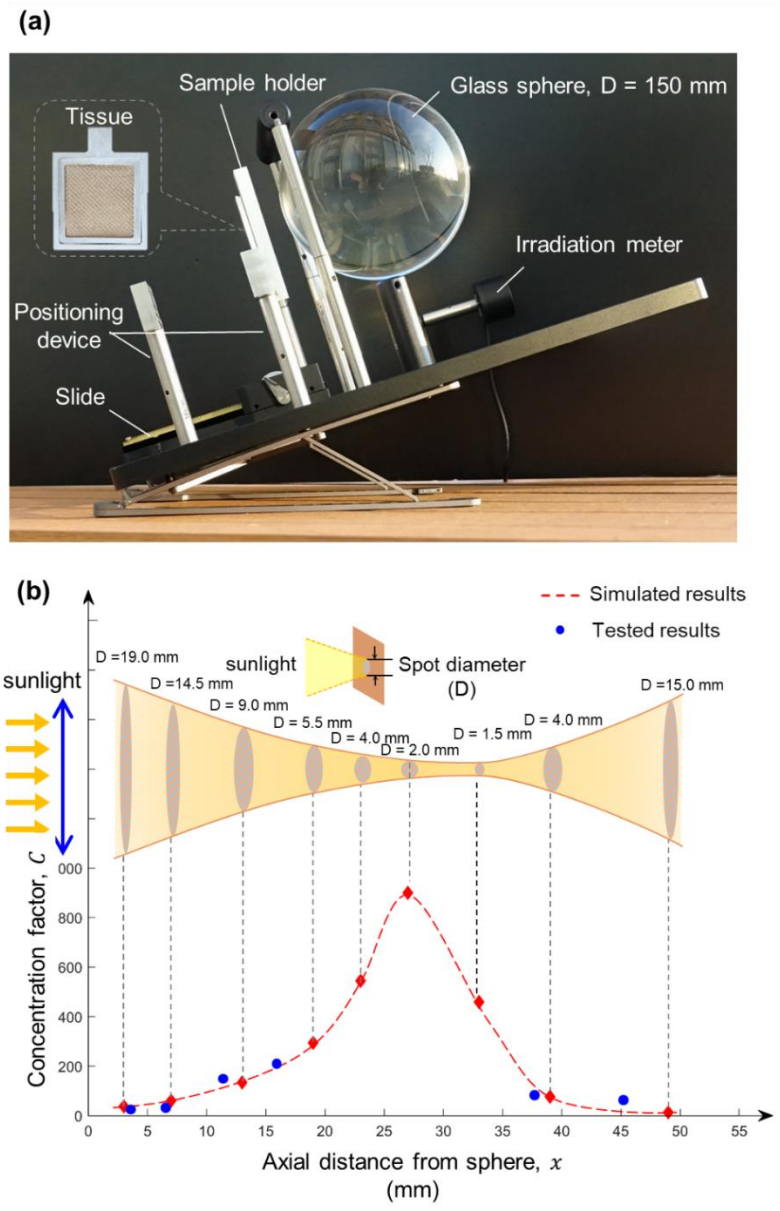

Figure 2- (a) Photos the experiment apparatus, and (b) overall concentration factor at different axial distance from sphere.

3. Experimental results

3.1. Smoldering ignition phenomena

Fig. 3a shows an example of a successful smoldering ignition process by a concentrated irradiation spot with a diameter of 1.5 mm and a resultant irradiation heat flux of 560 kW/m^2. Once the irradiation spot was applied on the sample surface, some smoke was released (Lin et al. 2019). Continuing the heating, the surface layer within the light spot turned black (or charred) and cracked, allowing the light beam to heat the lower layers directly. After heating for about 8 s, the sample detached from the apparatus but remained in the controlled environment (without wind) for another 5 min. As a result, the black spot expanded outwards evenly, expanding at a stable rate, and eventually burned out the sample. Fig. 3b shows an example of a failed smoldering ignition process by the concentrated irradiation spot with a diameter of 1.5 mm and a resultant radiant heat flux of 300 kW/m^2. Initially, smoke and a charring tendency were also observed. However, after heating for 8 s, no smoldering propagation phenomenon was observed, indicating a failed ignition.

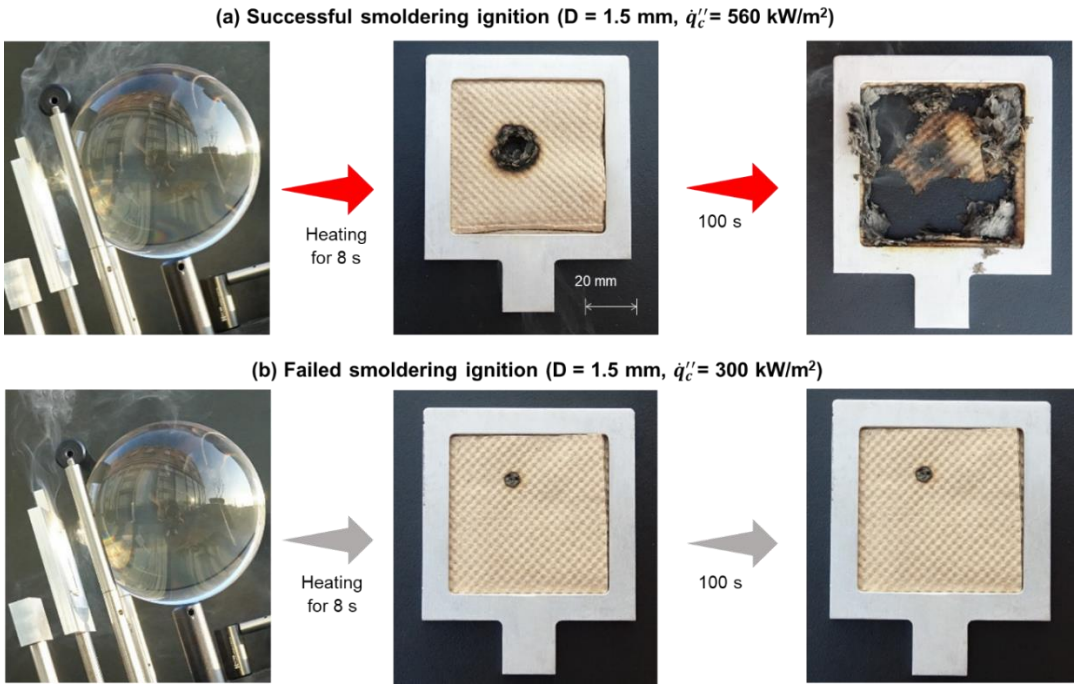

Figure 3- Smoldering ignition of dried tissue samples by concentrated irradiation spot with a diameter of 1.5 mm for 8 s, (a) successful ignition under irradiation of 560 kW/m², and (b) failed ignition under irradiation of 300 kW/m².

3.2. Critical heat flux

Fig. 4a plots the critical irradiation heat fluxes for smoldering ignition vs. the spot diameters. Interestingly, as the diameter of concentrated irradiation spot decreases from 20 mm to 1.5 mm, the critical heat flux increases dramatically from 18 kW/m^2 to 205 kW/m^2. Moreover, as the diameter of the irradiation spot increases, eventually, the critical heat flux for smoldering ignition approaches a near-minimum value obtained from the cone calorimeter (about 11 kW/m^2).

To scientifically understand the effect of the small irradiation spot on the critical heat flux of smoldering ignition, a simplified 2-D heat transfer analysis was applied. To achieve ignition, the critical irradiation heat flux ($\dot{q}''_{crt}$) should balance the environmental heat losses from the top and back sides ($\dot{q}''_{\infty}$) and the radial conductive heat loss to the virgin fuel ($\dot{q}''_{cond}$) (Lin et al. 2019; Huang and Gao 2020) a t the smoldering temperature (T_{sm}) as

$$\dot{q}''_{crt}\left(\frac{\pi D^2}{4}\right) = \dot{q}''_{\infty}\left(\frac{\pi D^2}{4}\right) \times 2 + \dot{q}''_{cond}(\pi D\delta) \qquad (2)$$

which can be further expressed and simplified as

$$\dot{q}''_{crt} = 2\dot{q}''_{\infty} + \frac{4\delta\dot{q}''_{cond}}{D} \quad \text{(small spot)} \qquad (3)$$

Therefore, as the diameter of the irradiation spot increases, the critical heat flux for smoldering ignition decreases, agreeing with the trend in Fig. 4a.

As the diameter of the irradiation spot (D) increases, the effect of conduction in Eq. (3) gradually approaches zero. Thus, for a larger irradiation spot, heat transfer can be approximated as a conventional 1-D process. The critical heat flux for smoldering ignition then approaches 11 kW/m^2, which approximately equals the environmental heat losses from the top and back surfaces as

$$\dot{q}''_{crt} = 2\dot{q}''_{\infty} = 2[\varepsilon\sigma(T_{sm}^4 - T_{\infty}^4) + h(T_{sm} - T_{\infty})] \quad \text{(large spot)} \qquad (4)$$

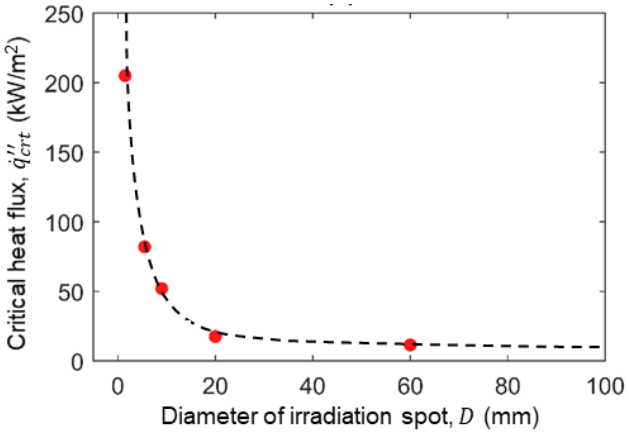

Figure 4-The relationship between diameters of irradiation spots (D) and critical ignition heat fluxes ($\dot{q}''_{crt}$).

4. Numerical modelling

To simulate the experimental observation, a 2-D numerical model is developed using Gpyro v0.8 (Lautenberger 2016). The governing conservation equations include the conservation of mass (Eq. 5), species (Eq. 6) and energy (Eq. 7) in the condensed phase as well as the mass (Eq. 8), species (Eq. 9), and momentum (Darcy's law) (Eq. 10) in the gas phase (see details in (Lautenberger 2016)). The schematic diagram of the computational domain has the same sample thickness (2 mm) and length (60 mm) as experiments. To save computational cost, the domain can be half of the actual sample owing to geometrical symmetry (Lin et al. 2022), as illustrated in Fig. 5.

$$\frac{\partial \bar{\rho}}{\partial t} = -\dot{\omega}'''_{fg} \quad (5)$$

$$\boldsymbol{\frac{\partial(\bar{\rho} Y_i)}{\partial t} = \dot{\omega}'''_{fi} - \dot{\omega}'''_{di}} \quad (6)$$

$$\boldsymbol{\frac{\partial(\bar{\rho}\bar{h})}{\partial t} = k\frac{\partial}{\partial x}\left(\frac{\partial T}{\partial x}\right) + k\frac{\partial}{\partial z}\left(\frac{\partial T}{\partial z}\right) + \dot{\omega}'''_{di}(-\Delta H_i)} \quad (7)$$

$$\frac{\partial}{\partial t}\left(\rho_g \overline{\psi}\right) + \frac{\partial \dot{m}''_x}{\partial x} + \frac{\partial \dot{m}''_z}{\partial z} = \dot{\omega}'''_{fg} \quad (8)$$

$$\frac{\partial}{\partial t}\left(\rho_g \overline{\psi} Y_j\right) + \frac{\partial}{\partial x}\left(\dot{m}''_x Y_j\right) + \frac{\partial}{\partial z}\left(\dot{m}''_z Y_j\right) = -\frac{\partial}{\partial x}\left(\overline{\psi}\rho_g D_{eff}\frac{\partial Y_j}{\partial x}\right) - \frac{\partial}{\partial z}\left(\overline{\psi}\rho_g D_{eff}\frac{\partial Y_j}{\partial z}\right) + \dot{\omega}'''_{fj} - \dot{\omega}'''_{aj} \quad (9)$$

$$\dot{m}''_z = -\frac{\kappa}{\nu}\frac{\partial p}{\partial z}\ \dot{m}''_x = -\frac{\kappa}{\nu}\frac{\partial p}{\partial x}\ \left(\rho_g = \frac{P\overline{M}}{RT}\right) \quad (10)$$

For the symmetrical plane ($x = 0$), adiabatic and impermeable boundary conditions are applied. At the top free surface ($z = 0$), initially ($t \le t_h$), irradiation ($\dot{q}''_{ir}$) with a heating diameter of $D/2$ is applied for a prescribed duration (t_h), and both convective ($h_{c,z=0} = 10\ \mathrm{W/m^2 \cdot K}$) and radiative heat losses are considered. Afterwards ($t > t_h$), the irradiation spot is removed. The mass transfer of gas species on the top free surface is considered. Based on the heat-mass transfer analogy, the mass transfer coefficient can be approximated as $h_{m,z=0} = h_{c,z=0}/C_g = 9.09\ \mathrm{g/m^2 \cdot s}$ (Lautenberger 2016). At the right and bottom boundary ($z = \delta$ and $x = L/2$), similar to the top free surface, both convective ($h_{c,z=0} = 10\ \mathrm{W/m^2 \cdot K}$) and radiative heat loss are considered, and the same mass transfer of gas species as the top surface is applied on the bottom surface. TThe whole computational domain has the same initial gas composition as the ambient air ($Y_{O_2} = 0.232$ and $Y_{N_2} = 0.768$). The solution starts to converge at $\Delta z = \Delta x = 0.1$ mm and $\Delta t = 0.01$ s.

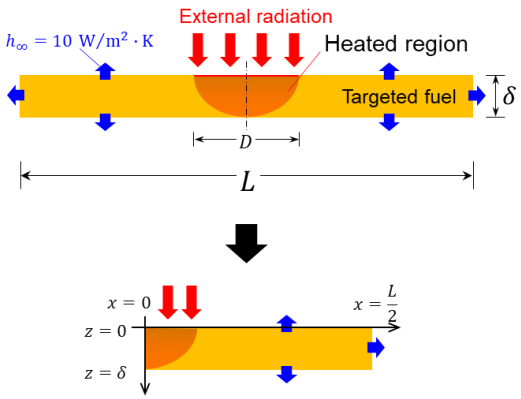

Figure 5- Schematic diagram of the 2-D computational domain for smoldering ignition using solar irradiation spots.

A previously developed 5-step kinetic scheme of typical biomass was applied here (Eq. 11-15) (Li et al. 2014; Yang et al. 2016; Huang et al. 2017). The kinetic parameters for the smoldering of biomass are obtained by optimizing the TG data in both inert and oxidative atmospheres using the Kissinger-Genetic Algorithm method ((Li et al. 2014)) and are listed in Table 1. The detailed species thermophysical properties can be found in (Huang et al. 2017).

$$\text{Water} \rightarrow \text{Water vapor} \quad [\text{dr}] \quad (11)$$

$$\text{Hemicellulose} \rightarrow \text{Char} + \text{Pyrolyzates} \quad [\text{hp}] \quad (12)$$

$$\text{Cellulose} \rightarrow \text{Char} + \text{Pyrolyzates} \quad [\text{cp}] \quad (13)$$

$$\text{Lignin} \rightarrow \text{Char} + \text{Pyrolyzates} \quad [\text{lp}] \quad (14)$$

$$\text{Char} + O_2 \rightarrow \text{Ash} + \text{gas} \quad [\text{co}] \quad (15)$$

Table 1- Chemical kinetic parameters and yields of 5-step reaction for biomass, where the reaction expression is $A_k + \nu_{O_2,k} O_2 \rightarrow \nu_{B,k} B_k + \nu_{g,k}$gas, and $\Delta H > 0$ is endothermic.

Parameter	*dr*	*hp*	*cp*	*lp*	*co*
$\lg Z_k$ (lg (s^{-1}))	8.12	8.2	11.4	21.4	12.9
E_k (kJ/mol)	67.8	106	154	229	184
n_k (-)	3	1.49	0.95	8.7	1.27
n_{k,O_2} (-)	0	0	0	0	1
$\nu_{B,k}$ (kg/kg)	0	0.24	0.27	0.40	0.06
ΔH_k (MJ/kg)	2.26	0.2	0.2	0.2	-20
$\nu_{O_2,k}$ (kg/kg)	0	0.5	0.5	0.5	1.5

5. Modelling results

Fig. 6(a) summarizes the modeled ignition time and compares it with the experimental data (uncertainty shown by shadowed area). Considering the complex nature of the smoldering process, a good agreement can be observed between predictions and experiments. Also, the effect of irradiation level ($\dot{q}''_{ir}$) on the ignition time is well predicted by the model; that is, the ignition time decreases as the irradiation level increases. For example, given an irradiation spot of 5 mm, as the radiant heat flux increases from 60 kW/m^2 to 150 kW/m^2, the predicted ignition time decreases from 85 s to 8 s.

Fig. 6(b) further summarizes the predicted minimum heat fluxes of smoldering ignition for different irradiation spots and compares them with the experimental data. For example, as the diameter of the irradiation spot increases from 2 mm to 10 mm, the predicted minimum heat flux for smoldering ignition decreases from

85 kW/m^2 to 43 kW/m^2. In general, simulations show an excellent agreement with experimental measurements with a relative error of less than 10%.

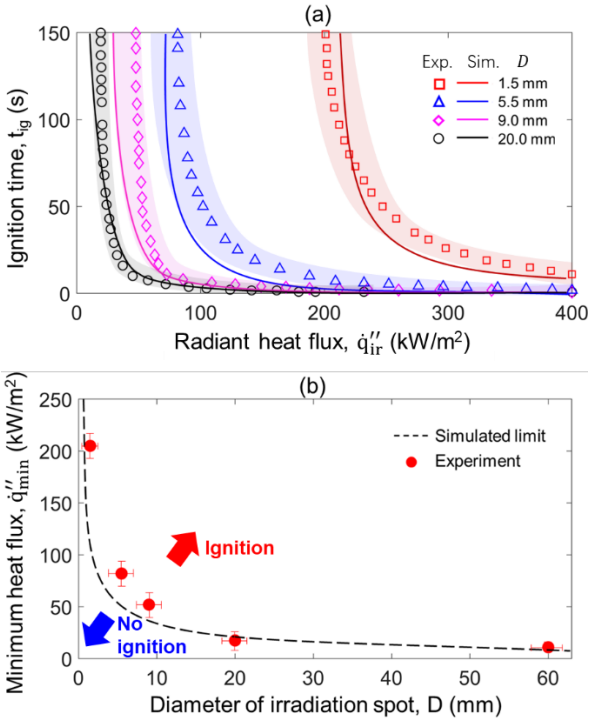

Figure 6- (a) Comparison between the experimental and modelled ignition time under different irradiation spots, (b) predicted minimum heat flux of smoldering ignition vs. test data.

6. Conclusion

In this work, we investigated the smoldering ignition of multi-layered thin tissue paper (common fuels in wildland abandoned by humans) by small irradiation spots. We found that the measured minimum spot irradiation for smoldering ignition is not constant but remains much higher than the 11 kW/m^2 measured from cone-calorimeter tests. As the diameter of irradiation spots decreases from 20.0 mm to 1.5 mm, the minimum irradiation necessary for smoldering ignition increases from 17.5 kW/m^2 to 205 kW/m^2. A simplified heat transfer analysis was proposed, which explains the critical smoldering ignition heat flux for solar irradiation spots by including two-dimensional cooling effects.

Afterwards, a 2-D computational model was successfully established to reproduce the experimental observations and validate the results. Future numerical simulations are needed to further reveal the underlying physical and chemical process of smoldering spot ignition for other fuels.

7. Acknowledgement

This research is funded by the National Natural Science Foundation of China (NSFC) No. 51876183.

8. Reference

Caton SE, Hakes RSP, Gorham DJ, Zhou A, Gollner MJ (2017) Review of Pathways for Building Fire Spread in the Wildland Urban Interface Part I: Exposure Conditions. Fire Technology 53, 429–473. doi:10.1007/s10694-016-0589-z.

Drysdale D (2011) 'An Introduction to Fire Dynamics.' (John Wiley & Sons, Ltd: Chichester, UK) doi:10.1002/9781119975465.

Fernandez-Pello AC (2017a) Wildland fire spot ignition by sparks and firebrands. Fire Safety Journal 91, 2–10. doi:10.1016/j.firesaf.2017.04.040.

Fernandez-Pello AC (2017b) Wildland fire spot ignition by sparks and firebrands. Fire Safety Journal 91, 2–10. doi:10.1016/j.firesaf.2017.04.040.

Huang X, Gao J (2020) A review of near-limit opposed fire spread. Fire Safety Journal 103141. doi:10.1016/j.firesaf.2020.103141.

Huang X, Li K, Zhang H (2017) Modelling bench-scale fire on engineered wood : Effects of transient flame and physicochemical properties. Proceedings of the Combustion Institute 36, 3167–3175. doi:10.1016/j.proci.2016.06.109.

Lautenberger C (2016) Gpyro-A Generalized Pyrolysis Model for Combustible Solids: Users'Guide. (Berkeley)

Li K, Huang X, Fleischmann C, Rein G, Ji J (2014) Pyrolysis of Medium-Density Fiberboard : Optimized Search for Kinetics Scheme and Parameters via a Genetic Algorithm Driven by Kissinger's Method. Energy & Fuels 28, 6130−6139. doi:10.1021/ef501380c.

Lin S, Sun P, Huang X (2019) Can peat soil support a flaming wildfire? International Journal of Wildland Fire 28, 601–613. doi:10.1071/wf19018.

Lin S, Yuan H, Huang X (2022) A Computational Study on the Quenching and Near-Limit Propagation of Smoldering Combustion. Combustion and Flame 238,. doi:10.1016/j.combustflame.2021.111937.

Rein G (2014) Smoldering Combustion. SFPE Handbook of Fire Protection Engineering 2014, 581–603. doi:10.1007/978-1-4939-2565-0_19.

Santoso MA, Christensen EG, Yang J, Rein G (2019) Review of the Transition From Smouldering to Flaming Combustion in Wildfires. Frontier in Mechanical Engineering 5,. doi:10.3389/fmech.2019.00049.

TracePro Software for design and analysis of illumination and optical systems.

Wang S, Lin S, Liu Y, Huang X, Gollner MJ (2022) Smoldering Ignition using a Concentrated Solar Irradiation Spot. Fire Safety Journal 129,. doi:10.1016/j.firesaf.2022.103549.

Yang J, Chen H, Zhao W, Zhou J (2016) TG-FTIR-MS study of pyrolysis products evolving from peat. Journal of Analytical and Applied Pyrolysis 117, 296–309. doi:10.1016/j.jaap.2015.11.002.